Hydrogenated caged clusters of Si, Ge, and Sn and their endohedral doping with atoms: *Ab initio* calculations

Vijay Kumar[1,2,3] and Yoshiyuki Kawazoe[3]
[1]*Dr. Vijay Kumar Foundation, 45 Bazaar Street, K. K. Nagar (West), Chennai 600 078, India*
[2]*Research Institute for Computational Sciences (RICS), National Institute of Advanced Industrial Science and Technology (AIST), AIST Tsukuba Central 2, Umezono 1-1-1, Tsukuba 305-8568, Japan*
[3]*Institute for Materials Research, Tohoku University, Aoba-ku, Sendai 980-8577, Japan*
(Received 6 February 2007; published 20 April 2007)

We report results of an *ab initio* study on the stability of hydrogenated empty cages X_nH_n with X=Si, Ge, and Sn, and n=8, 10, 12, 14, 16, 18, 20, 24, and 28. All these cages have large highest-occupied–lowest-unoccupied molecular orbital (HOMO-LUMO) gaps. The HOMO-LUMO gap for Ge cages is found to be even larger than the values for Si cages, though in bulk Ge has a smaller band gap than Si. Cages with n=16 and 20 are found to be particularly stable in the form of fullerene structures. The bonding in the dodecahedral $X_{20}H_{20}$ cage is very close to sp^3 type and it leads to the highest stability of this cage with perfect icosahedral symmetry. Endohedral doping of the empty cages such as Si_nH_n (n=10–28), with different guest atoms shows that doping can be used to manipulate the HOMO-LUMO gap with the possibility of varying their optical properties as well as to prepare species with large magnetic moments. Depending upon the guest atom, the character of the HOMO and the LUMO states and their origins either from the cage or the guest atom changes. This could lead to their applications in sensors. In contrast to the metal-encapsulated silicon-caged clusters, the embedding energy of the guest atom in the hydrogenated silicon fullerenes is small in most cases due to the weak interactions with the cage and therefore these slaved guest atoms can keep their atomic properties to a large extent. We find that atoms with closed electronic shell configurations such as Ca, Ba,… generally occupy the center of the cage. However, Be and other open electronic shell atoms tend to drift towards the wall of the cage. Doping of halogens such as iodine and alkalis such as Na can be used to produce, respectively hole and electron doping while transition-metal atoms such as V, Cr, Mn, and Fe are shown to produce atomiclike magnetic moments in many cases. In most of these cases the HOMO-LUMO gap becomes small because the guest atom orbital(s) are only partially occupied. However, for Ni and Zn the HOMO-LUMO gap is large as the hybridized d orbitals become fully occupied. An interesting finding is that the endohedral doping can lead to a higher-energy undoped cage isomer to become the lowest-energy doped isomer. Implications of this result for endohedral fullerenes of carbon are also discussed.

DOI: 10.1103/PhysRevB.75.155425 PACS number(s): 73.22.−f, 36.40.Cg, 61.46.−w, 61.48.+c

I. INTRODUCTION

Recent predictions of metal-encapsulated caged clusters of silicon,[1,2] germanium,[3–6] tin,[4–7] and lead,[6] as well as their realization in the laboratory,[8–15] have opened up new avenues to develop different nanostructures of silicon and other materials that could be attractive for miniature devices and in optoelectronic, magnetic, sensor, catalytic, and other applications. Large abundances of 15 and 16 Si atom charged clusters doped with a Ti,[10] Cr, Mo, or W (Ref. 8) atom, ten-atom anion clusters of Ge and Sn doped with a Co (Ref. 11) atom, and ten and 12-atom cation clusters[13] of Pb doped with an Al atom as well as different abundances of clusters of tetravalent elements Si, Ge, Sn, and Pb with the same dopant,[14] lend support to the idea[1] that metal encapsulation provides strong size selectivity to these clusters. The enhanced stability and size selectivity of the elemental clusters by metal doping could lead to their production in macroscopic quantities and the development of their assemblies. Recently, high abundance of neutral $Si_{16}Ti$ has been obtained[12] almost exclusively supporting the prediction[1] of the magic behavior of this cluster with closed electronic and atomic shells. Also, the prediction[5] of the magic behavior of Zn-and Mn-doped Sn_{12} clusters has been confirmed.[14] Further studies of H interaction with such clusters have led[16] to the predictions of empty cage Si_nH_n fullerenes in which H atoms are used to terminate the dangling bond of each Si atom in the fullerene cage. These cage structures are different from most other studies on hydrogenated silicon clusters where the number of H atoms is generally not equal to the number of Si atoms. In such studies hydrogen is used to passivate a bare silicon nanoparticle, which is generally assumed to have the bulk diamond structure. Recent experiments[17] suggest that Si_nH_n clusters can be produced in the laboratory by proper control of temperature and relative fractions of Si and H atoms. Here we present a detailed study of Si_nH_n cages with n=8, 10, 12, 14, 16, 18, 20, 24, and 28 and also show that similar structures are stable for Ge and Sn. Many of these cages can be doped with a guest atom to develop endohedral cages of Si, Ge, and Sn similar to the endohedral fullerenes of carbon,[18] but the former are stabilized by H capping.

Recently, endohedral doping of F, Cl, Br, and I anions in the $Si_{20}H_{20}$ cage has been studied.[19] While all these atoms fit well in the cage, the Br anion has been found to have just the right size so that the cage has no significant change. Anion templates have been used to produce a variety of species and this could be a very effective way for the large-scale production of endohedral silicon fullerenes. Following these devel-

opments, Zhang *et al.*[20] have studied the stability of endohedral doping of neutral and cations of Li, Na, K, Be, Mg, and Ca in the $Si_{20}H_{20}$ cage. Also, exohedral doping of the $Si_{20}H_{20}$ dodecahedral cage has been found[21] to leave the cage as well as the highest-occupied–lowest unoccupied molecular orbital (HOMO-LUMO) gap nearly unchanged. This is interesting for the fuctionalization of such cages as well as for the development of other derivatives. Another interesting aspect of the endohedral cages is their different behavior compared with the metal-encapsulated Si, Ge, Sn, and Pb clusters.[22,23] In the latter case the magnetic moment of the doped atom is generally quenched. However, endohedral doping of hydrogenated cages could provide a way to produce nanospecies with large magnetic moments due to the much weaker interaction of the endohedral atom with the cage. The HOMO-LUMO gap could as well be tailored to obtain desired optical and electronic properties.

Structurally $Si_{20}H_{20}$ is similar to dodecahedrane $C_{20}H_{20}$, which is used[24] as a precursor to form C_{20} fullerene in the laboratory. Several other C_nH_n hydrocarbon species such as C_6H_6 prismane, C_8H_8 cubane, and $C_{10}H_{10}$ pentaprismane have been synthesized. It can therefore be expected that similar species of silicon and other group 14 elements could be produced. Earley[25] has calculated strain in polyhedrane clusters X_nH_n, X=Si, Ge, and Sn, and n=4, 6, 8, 10, 12, 16, 20, and 24 depending upon the type of rings present in the clusters and found that n=20 fullerene is the least strained. Endohedral and exohedral complexes of $C_{20}H_{20}$ have also been studied[26] while endohedral doping in smaller hydrocarbon cage complexes has been explored theoretically.[27] Furthermore Si-H could be effectively replaced with P. Accordingly similar cages of P can be expected. Indeed P_{20} has been shown[28] to be a very stable cage that can also accommodate endohedral atoms or ions.

From an experimental point of view, endohedral doping of carbon fullerenes[18] such as C_{60}, C_{82}, and C_{84} has been extensively studied and a variety of guest atoms or clusters have been inserted in the cage. Crystals[29] and peapods[30] of endohedral carbon fullerenes have also been prepared. The latter are arrays of endohedral carbon fullerenes in carbon nanotubes. By endohedral as well as endohedral-exohedral doping of C_{28} fullerene cage species such as $Ti@C_{28}H_4$ have been suggested[31] to be stable. With empty cage Si fullerenes, it may be possible to prepare a new variety of Si nanospecies and their assemblies. Empty Si_{20} and Si_{24} or Si_{28} fullerene cages are found in bulk clathrates[32] such as Si_{46} or Si_{136}, respectively. Similar clathrate structures of Ge and Sn have been developed[33] as well. The fullerene cages in these structures are interlinked so that each Si, Ge, or Sn atom is fourfold coordinated. The cages can be occupied by guest atoms such as Ba (Ba_8Si_{46}) and Na (Na_8Si_{46}). Doping of the cages in these forms of silicon can lead to even larger band gaps[34] than the value for bulk Si. As an example, Xe-doped clathrates are predicted[34] to be photoluminescent in the visible range. Another interesting property of the doped clathrates is the occurrence of superconductivity.[34,35] In hydrogenated Si fullerenes, each Si has three neighboring Si atoms and a capping H atom[16] so that all the valence electrons of Si atoms are shared giving rise to their stability and large HOMO-LUMO gaps. Thus H atoms effectively have the same role as links found between cages in clathrate compounds. Therefore, the study of the doping of such fullerene cages cannot only lead to new nanospecies of Si, Ge, and Sn with interesting optoelectronic and magnetic properties but also to new possibilities of dopants in clathrates as well as help to understand their properties from a local point of view.

In Sec. II we present the method of calculation. The results are discussed in Sec. III while a summary and concluding remarks are given in Sec. IV.

II. METHOD OF CALCULATION

We use *ab initio* ultrasoft pseudopotential plane-wave method[36] and generalized gradient approximation[37] for the exchange-correlation energy. The cluster is placed in a large simple cubic unit cell of side up to 20 Å. The Γ point is used for the Brillouin-zone integrations. The structures are optimized using the conjugate gradient method without any symmetry constraint. We consider Si_nH_n cage clusters with n, an even number ranging from 8 to 20, 24, and 28. Some results are also given for n=6. The starting atomic configurations have been chosen from a few geometries such as cube, decahedron, and fullerene structures. Stabilities of the structures have been checked by displacing the ions from their equilibrium positions. Similar calculations have been done for Ge and Sn clusters also. Selected clusters of silicon are doped with guest atoms as representatives of these systems. Guest atoms such as Ar, Xe, and divalent metal atoms with closed electronic shells as well as those with an open electronic shell such as alkalis, halogens, and transition-metal atoms, have been considered. In the latter cases the cluster has a net spin magnetic moment and the calculations have been done using the spin-polarized exchange-correlation functional without imposing any constraint such as symmetry and spin multiplicity. In some cases spin isomers have also been calculated to check the configuration with the lowest energy. For the case of Ar and Xe, calculations have been performed using the projector augmented wave (PAW) method.[38] The embedding energy (EE) of the guest atom, defined as the negative of the difference in energy of the endohedral hydrogenated Si fullerene and the isolated guest atom plus the empty cage, is much smaller ($\approx$1 eV) in most cases as compared to $\approx$10 eV in metal-encapsulated Si clusters.[1] This leads to the interesting magnetic behavior of these species. Further analysis of the cage orbitals of Si_nH_n and Ge_nH_n has been done using the Gaussian program[39] with the B3PW91 hybrid exchange-correlation functional and by analyzing the site and angular momentum decomposed contributions to the electronic spectra within the plane-wave method. In the Gaussian method we used 6-311+G* basis set for Si and SDD basis set for Ge cages.

III. RESULTS

A. Empty cages

Figure 1 shows the optimized structures for Si_nH_n clusters. These have symmetric structures such as prism (D_{3h}), cube (O_h), and decahedron (D_{5h}) for n=6, 8, and 10, respectively very similar to C_nH_n molecules. For Si_6H_6 another

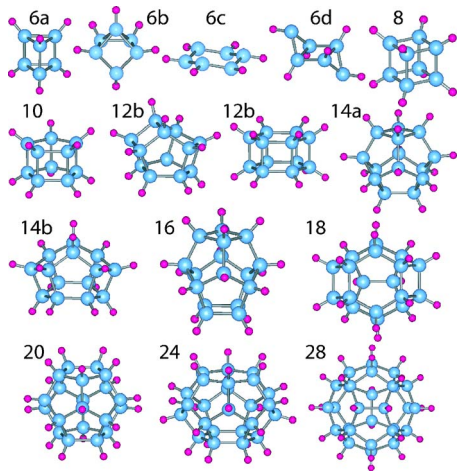

FIG. 1. (Color online) Optimized structures of Si_nH_n with $n=6-20$ (even number), 24, and 28. Red (blue) balls represent H (Si) atoms and the numbers, the value of n. Alphabets a,b,… represent isomers with increasingly higher energies.

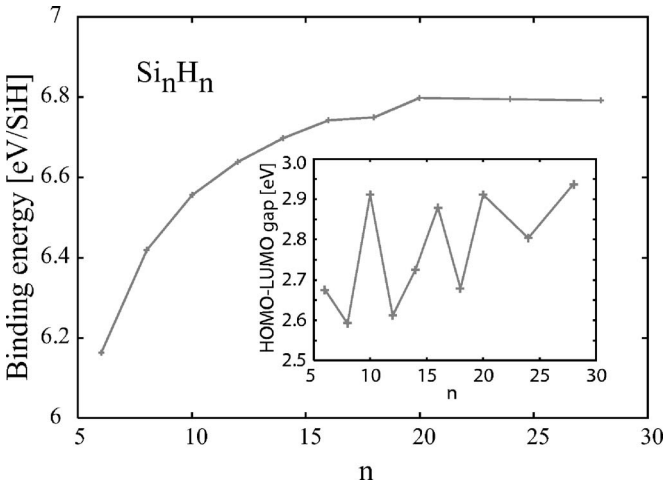

FIG. 2. Binding energy (BE) per SiH unit and (inset) the HOMO-LUMO gap for Si_nH_n clusters. A slight decrease in the BE beyond $n=20$ can be noticed. The HOMO-LUMO gap for $n=10$, 16, 20, and 28 shows a local maximum.

structure (6b) based on capping of a bent pentagon geometry of Si_6 is nearly degenerate with the prism isomer. In the latter case, the deviation from sp^3 bonding is significant and the strain energy is quite large.[25] Two ring structures (6c and 6d) for Si_6H_6 lie 0.63 and 1.34 eV higher in energy, respectively, suggesting the preference for a higher coordination isomer. Si_8H_8 has the cubane structure (8) while the decahedral structure of $Si_{10}H_{10}$ is shown in Fig. 1 (10). Structures for clusters with $n=12$, 16, and 20 were reported earlier.[16] However, the hexagonal prism D_{6h} cage (12b) for $n=12$ is not the ground state[22] and an isomer with four pentagons and four rhombi (12a) with D_{2d} symmetry lies 1.11 eV lower in energy. In this case two pairs of rhombi are isolated, which is energetically favorable as rhombi create strain in the preferred sp^3 bonding in silicon. This isomer also has a 2.61 eV HOMO-LUMO gap as compared to the value of 2.56 eV for the hexagonal prism isomer. This result also shows that fullerenelike cages with pentagons are more favorable[40] than cages with hexagons. Earley[25] also obtained lower strain in the D_{2d} structure of $Si_{12}H_{12}$. The smallest fullerene of carbon, C_{20}, has twelve pentagonal faces. For a smaller number of atoms some pentagons need to be eliminated and rhombi or triangular faces become necessary. We call smaller-size structures to be fullerenelike if the number of nearest neighbors on the cage for each atom is three (leaving aside the H atom).

Empty cage fullerenelike structures are obtained for $n=14$. An isomer with a hexagon and nearest- neighbor rhombi (14b) is 0.41 eV higher in energy as compared to another threefold symmetric isomer that has six pentagons and three isolated rhombi (14a) confirming again that structures with pentagons and isolated rhombii are more favorable and follow the isolated rhombus rule[40] rather than the isolated pentagon rule in carbon fullerenes. A fullerenelike structure (16 and 18) has also been obtained for $n=16$ (D_{4d}) and 18 while cages with $n=20$, 24, and 28 are the same as for carbon fullerenes with I_h, D_{6h}, and T_d symmetries (20, 24, and 28 in Fig. 1), and with 0, 2, and 4 hexagons, respectively, besides 12 pentagons. Earley[25] considered a cage with O_h symmetry for $Si_{24}H_{24}$ having square and hexagonal faces. However, it has higher-strain energy as compared to the fullerene structure. This is because both squares and hexagons create strain in sp^3 bonding. The $n=16$ cage [Fig. 1 (16)] has two square faces that are far apart from each other and this reduces strain in the structure. This is one of the most stable fullerenelike isomers. In order to further check the stability of the cages, we displaced silicon atoms considerably from their equilibrium positions randomly for $n=12$, 14, 16, and 20 cages. However, after reoptimization, all the cages relaxed back to their equilibrium structures, suggesting that the cage structures are stable and represent the minimum-energy structures of these clusters. These results are in contrast to most previous studies[41,42] of hydrogen-terminated silicon clusters in which a fragment of bulk silicon is assumed and the dangling bonds are terminated by hydrogen. Pichierri *et al.*[21] have shown that for the $Si_{20}H_{20}$ cage the ionization potential is high (8.10 eV) and the electron affinity, low (1.54 eV) compared with the corresponding values of 7.58 and 2.67 eV for C_{60}, respectively. These results also reflect the high stability of the fullerene cages of silicon.

The binding energy (BE) of the cages, defined with respect to free atoms, increases monotonically until $n=20$ (Fig. 2) beyond which there is a slight decrease. Cages with $n=16$ and 20 are particularly stable. The HOMO-LUMO gap also has a local maximum value ($\approx 2.895 \pm 0.015$ eV) for cages with $n=10$, 16, and 20. The HOMO-LUMO gap for $n=24$ and 28 cages is 2.80 and 2.94 eV, respectively. The high value for $n=28$ is due to the tetrahedral symmetry of this cage. The nearly constant value of the HOMO-LUMO gap for different n is interesting as samples even with a mixture of clusters of different sizes may have similar optical properties. It is noteworthy that experiments[17] on $Si_{14}H_x$ clusters at different temperatures showed a maximum in the abundance distribution for $x=14$ at around 700 K. A cage structure similar to the higher-energy isomer obtained by us

(14b in Fig. 1) was suggested[17] for this cluster. Our calculations show that the second-order difference in energy among the even n cages is nearly zero for the $Si_{14}H_{14}$ fullerene cage (see nearly linear behavior of the BE between $n=12$ and 16 in Fig. 2) and therefore in the family of Si_nH_n cages, the $n=14$ cage is not magic and we do not expect it to be highly abundant. Note that in experiments[17] there is a somewhat broad distribution of $Si_{14}H_x$ clusters as a function of x and the maximum occurs at $x=14$. On the other hand, cages with $n=16$ and 20 are particularly stable and magic. Therefore it can be expected that these cages would show strong abundances.

Cages with $n=16$ and 20 are large enough to accommodate a variety of guest atoms similar to the carbon fullerenes. The inner diameter of the $Si_{20}H_{20}$ cage is similar to that of C_{60}, which has been doped endohedrally by different atoms. Therefore there are interesting possibilities for the formation of endohedrally doped silicon fullerenes. The bonding nature in Si_nH_n cages is predominantly sp^3 type. For larger cages with $n>20$, the sp^2 component in the bonding increases due to the presence of hexagons and it is likely to be the reason for the decrease in the BE for $n>20$ as sp^2 bonding is not favored by silicon. Thus hexagons are defects in the fullerene cages of silicon unlike carbon for which pentagons are the places of strain. Thus our results suggest the highest stability of the $n=20$ fullerene cage of Si_nH_n with all pentagonal faces and highest (icosahedral) symmetry. Note that the icosahedral $Th@Si_{20}$ fullerene also has the highest binding energy[43] among the metal-encapsulated silicon clusters.

Similar calculations have been carried out for Ge and Sn cages with hydrogen termination. As Ge and Sn clathrates also exist,[33] it is of interest to study the stability of hydrogen-terminated cage structures of Ge and Sn also. For $n=6$, we find that the pentagonal isomer becomes 0.50 and 0.46 eV lower in energy for Ge and Sn, respectively, as compared to the prism isomer. For larger values of n we explored the stability of the cage structures. For $n=8$ and 10, cubane and decahedral isomers, respectively, and for $n=12$ and 14 fullerenelike cages are stable for Ge and Sn as is the case for silicon. The $n=12$ cage of Ge was also distorted randomly so that the energy of the starting configuration increased by about 11 eV, but the structure came back to the same cage giving us confidence that the cage structure was indeed stable. Similarly the $n=16$ and 20 cages were distorted so that the initial structures had about 16 and 4 eV higher energy, respectively. But after reoptimization we obtained the relaxed structures to be the same as the cage structures. The BE of Ge and Sn cages are lower as compared to those of Si (Table I). However, interestingly the HOMO-LUMO gaps for Ge cages are larger than the values for the Si cages whereas for Sn, these are slightly lower (Table I). The higher HOMO-LUMO gaps[44] for Ge cages make them attractive for optical absorption in the ultraviolet range and these could be interesting for applications such as developing coatings for skin cancer protection. Cages with $n=10$, 16, and 20 are again magic. The HOMO-LUMO gaps for these cages also have local maximum values similar to Si cages. The BE decreases slightly after $n=20$, and this suggests that in all cases, the $n=20$ cage is the best. However, the change in energy becomes smaller in the case of Sn. Therefore the strain in Sn structures is minimal as it was also found by Earley.[25]

TABLE I. Binding energy (BE) in eV/(XH) and HOMO-LUMO gap (eV) for X_nH_n, X=Si, Ge, and Sn cages.

	Si		Ge		Sn	
n	BE	Gap	BE	Gap	BE	Gap
6	6.160	2.676	5.302	2.173	4.603	1.654
8	6.417	2.592	5.468	2.958	4.736	2.377
10	6.555	2.911	5.611	3.210	4.859	2.734
12	6.637	2.612	5.677	3.130	4.906	2.466
14	6.697	2.725	5.735	3.243	4.952	2.620
16	6.741	2.880	5.777	3.344	4.987	2.702
18	6.749	2.679	5.783	3.118	4.992	2.489
20	6.798	2.911	5.830	3.338	5.029	2.700
24	6.795	2.804	5.826	3.171	5.028	2.549
28	6.791	2.937	5.823	3.262	5.026	2.561

The nearest-neighbor bond lengths in Si, Ge, and Sn cages are given in Table II. These are in the range of 2.35–2.38 Å for Si cages, 2.45–2.50 Å for Ge cages, and 2.82–2.87 Å for Sn cages. The variation in bond lengths is small for different cages. The bond lengths compare well with the experimental values in the corresponding bulk, which are 2.35, 2.45, and 2.81 Å for Si, Ge, and Sn, respectively. The electronic spectra of X_nH_n, X=Si, Ge, and Sn cages are shown in Fig. 3 for $n=8-28$. The general features

TABLE II. Nearest-neighbor bond lengths in Å for X_nH_n, X=Si, Ge, and Sn lowest-energy cages.

n	Si	Ge	Sn
8	2.380	2.496	2.866
10	2.374, 2.380	2.484, 2.493	2.857, 2.864
12	2.353, 2.373, 2.382	2.455, 2.479, 2.491	2.828, 2.851, 2.863
14	2.357, 2.367, 2.372	2.458, 2.466, 2.475	2.832, 2.837, 2.846
16	2.359, 2.365, 2.374	2.458, 2.465, 2.479	2.829, 2.836, 2.851
20	2.364	2.460	2.830
24	2.355, 2.365, 2.370	2.452, 2.464, 2.468	2.822, 2.835, 2.839
28	2.359, 2.365, 2.368	2.457, 2.462, 2.469	2.828, 2.833, 2.840

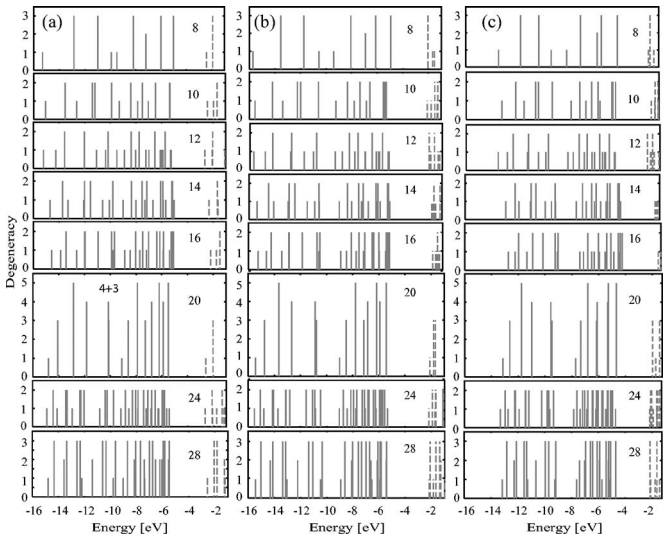

FIG. 3. (a) Electronic energy spectra of Si_nH_n clusters. The numbers indicate the size of the cage. In some cases the energies lie very close. One such case has been indicated as 4+3 in the case of $n=20$. (b) and (c) show the same as in (a) but for Ge_nH_n and Sn_nH_n, respectively. Broken lines denote the unoccupied states.

in the spectra for Si and Ge (also Sn) cages are similar except for small shifts in the energies of the states. An interesting finding in these nanosystems of Si and Ge is that the HOMO-LUMO gap for Ge cages ($n=8-28$) is larger[44] as compared to Si cages (see Table I) though in bulk the band gap for Ge is smaller than for Si. For Si, the LUMO is nondegenerate in all cases. It was shown[21] in the case of $Si_{20}H_{20}$ that the LUMO is localized inside the cage while the HOMO has large weight on the cage. This is important for exohedral and endohedral dopings of the cages. As we shall show below, the HOMO and the LUMO states, and therefore the optical properties of these cages, can be modified by doping in order to design materials with desired properties. For Ge cages while the HOMO is nearly at the same position as in Si cages, the LUMO shifts towards lower binding energy and therefore the HOMO-LUMO gap of Ge cages increases as compared to Si cages. In some cases the LUMO+1 state of Si cages becomes the LUMO for Ge cages. Accordingly, the LUMO in such Ge cages originates from the cage and therefore the effects of doping on Ge cages can be expected to be different as compared to Si cages. This has been demonstrated in Fig. 4, which shows the HOMO and LUMO of Si and Ge cages. In all cases the HOMO of Si and Ge cages originates from the cage. However, for Si, the LUMO has a large weight inside the cage. On the other hand, for Ge cages, the LUMO also originates from the cage. In most cases there is a high density of states near the HOMO and this can be important for the interaction of the cages with other species as well as for the assembly of the cages. The bonding nature in all these cages is dominantly covalent. In the case of Sn cages the largest HOMO-LUMO gap is obtained for $n=10$.

B. Endohedral doping of cages

We consider hydrogenated silicon cages for exploring endohedral doping. In small cages such as $Si_{10}H_{10}$ the guest

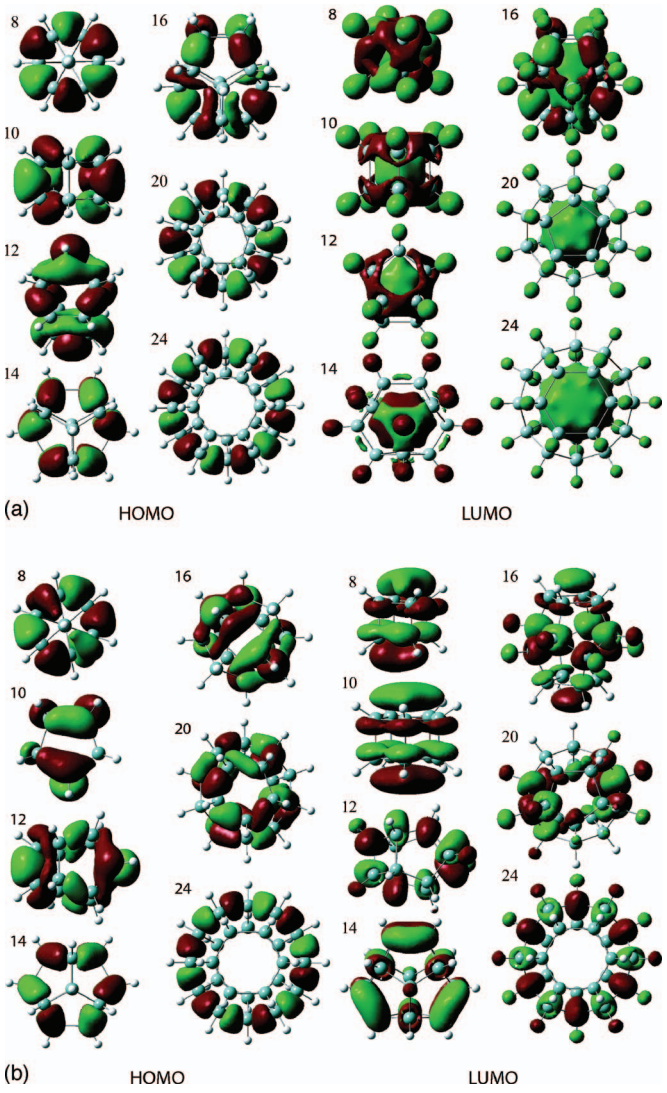

FIG. 4. (Color) Surfaces at 0.025 of highest-occupied molecular orbital (HOMO) and lowest-unoccupied molecular orbital (LUMO) of (a) Si_nH_n and (b) Ge_nH_n cages. The numbers denote n. White (blue) balls represent H (Si or Ge) atoms.

atom generally comes out but in larger cages different atoms can be endohedrally doped. In the following we describe these results.

1. $Si_{10}H_{10}$

For the $n=10$ cage, we tried relatively smaller atoms among the transition metals and found that after optimization Cr, Mn, Fe, and Ni atoms come out of the cage [Figs. 5(a)–5(d) for Cr, Mn, Fe, and Ni, respectively] in order to optimize M-Si interactions even though some Si-Si bonds become elongated. In the case of Ni doping, the cage has fivefold rotational symmetry and Ni atom caps a pentagonal face of Si atoms. The magnetic moments for Cr, Mn, Fe, and Ni cases are 4, 3, 2, and $0\mu_B$ while the HOMO-LUMO gaps are 1.38, 0.67, 0.78, and 1.94 eV, and the EEs, 1.37, 1.55, 3.37, and 4.80 eV (Fig. 6), respectively. In the case of Cr and Mn atom doping the exchange-splitting is large and a reduction in the magnetic moment compared to the atomic values

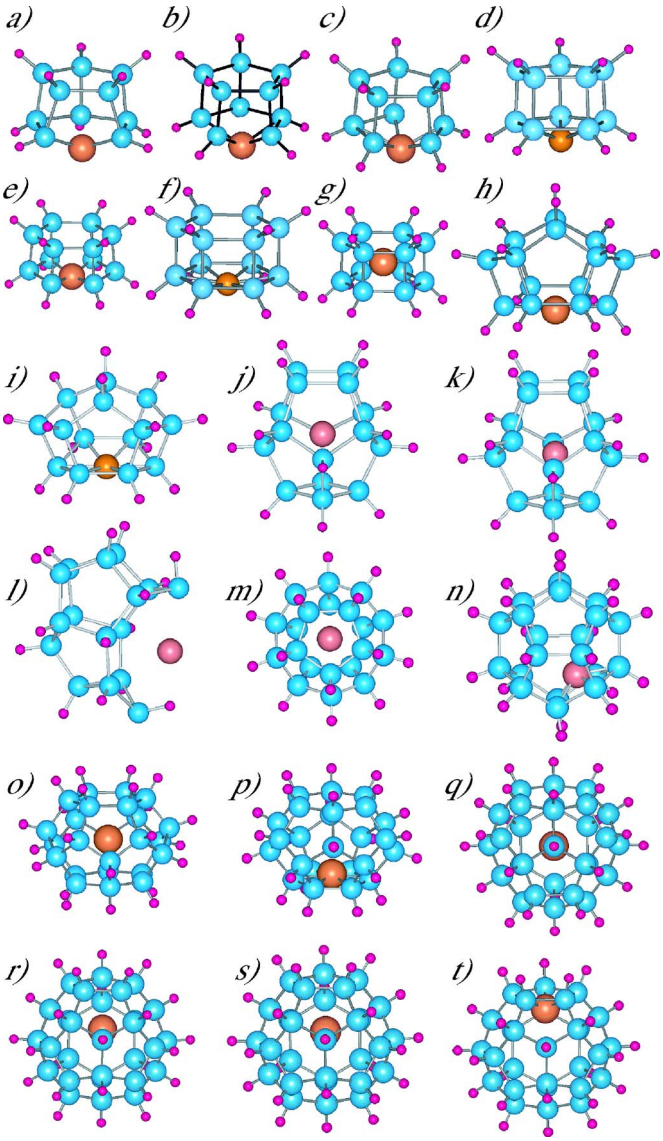

FIG. 5. (Color online) Structures of doped Si_nH_n cages. (a) Cr, (b) Mn, (c) Fe, (d) Ni in the $n=10$ cage; (e) Fe or Mn, (f) Ni, and (g) Ti in the $n=12$ cage; (h) Cr or Fe and (i) Mn in the $n=14$ cage; (j) Be, Ca, Cr, Mn, V, Zn, or Ar, (k) Fe, and (l) Ba in the $n=16$ cage; (m) Ar, Xe, Ba, Ca, Cr, Fe, Mn, Mo, and Zn, and (n) Be in the $n=20$ cage; (o) Ba, Ca, Cr, Mn, Xe, Zn, and Ar, and (p) Be in the $n=24$ cage; and (q) Ar, Ba, Xe, (r) Zn, (s) Ca, and (t) Be in the $n=28$ cage. In the case of Ba in the $n=16$ cage, the cage is broken. In the case of the same figure for different dopants, there could be small variations in the bond lengths and these should be considered as representatives.

leads to a large reduction in the EE. The HOMO-LUMO gap for Ni doping is large and this cluster is likely to have interesting optical properties in the visible range. The angular momentum decomposition of the electronic states shows that the HOMO and LUMO for Cr, Mn, and Fe doping have dominant contributions from the $3d$ orbitals of the metal atom, which hybridize with the orbitals of the cage giving rise to a significant value of the EE and a small HOMO-LUMO gap. In the case of Cr a larger exchange splitting gives rise to a higher HOMO-LUMO gap. For Ni the hybridized $3d$ orbitals are fully occupied and the LUMO does not have the $3d$ character of Ni. This leads to a large HOMO-LUMO gap and zero magnetic moment on this cage.

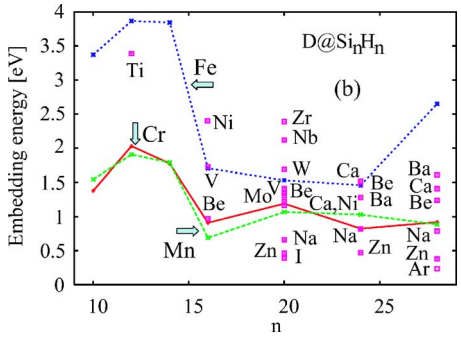

FIG. 6. (Color online) Embedding energies for various dopants D in Si_nH_n cages. The curves correspond to Fe, Cr, and Mn doping while the points correspond to other dopants.

2. $Si_{12}H_{12}$

For $n=12$, interestingly the hexagonal prism isomer, which is higher in energy without doping becomes lower in energy after doping as compared to the fullerene isomer. This finding could also have important implications for the study of the endohedral dopings of carbon fullerenes. Our results show that *a higher-energy isomer may interact with a dopant better and lower the energy of the doped system.* In an earlier study, Cr in $n=12$ hexagonal prism structure was found[16] to also come out of the cage slightly above a hexagon in order to optimize interactions with the Si atoms. This is because the $Si_{12}H_{12}$ cage is slightly oversized and Cr is not optimally bonded at the center. It also has $4\mu_B$ magnetic moment as compared to zero for $Si_{12}Cr$ due to the weakening of the interaction between the Cr atom and the hydrogenated silicon cage. The HOMO-LUMO gap is significant with the value of 0.93 eV. A similar behavior is obtained for Mn and Fe [Fig. 5(e)], which have 3 and $2\mu_B$ magnetic moments, 0.18 and 0.59 eV HOMO-LUMO gap, and 1.90 and 3.87 eV EE (Fig. 6), respectively. A nickel atom also comes out of the $n=12$ hexagonal prism cage and lies slightly above a hexagonal face [Fig. 5(f)]. It has sixfold rotational symmetry and zero magnetic moment. Similar to $Si_{10}H_{10}$, there is a large HOMO-LUMO gap of 1.72 eV. The EE is also large (5.01 eV). However, Ti, a larger atom remains inside the hexagonal cage [Fig. 5(g)]. It is to be noted that without H capping, the Ti atom creates significant strain[45] in the hexagonal prism isomer. The EE of a Ti atom in the cage is 3.39 eV and the HOMO-LUMO gap is relatively small (0.67 eV) due to the partial occupation of the $3d$ orbitals. The magnetic moment on this Ti-doped cluster is $2\mu_B$ as compared to the calculated value of $4\mu_B$ for an isolated Ti atom. In all these cases the magnetic moment of the metal atom is quenched by $2\mu_B$ due to interaction with the cage. However, in the fullerenelike cage of $Si_{12}H_{12}$ the magnetic moment of a Ti atom remains $4\mu_B$. The interaction energy of a Ti atom with the $n=12$ fullerene cage is less by 1.41 eV than in the hexagonal prism structure. Therefore, the hexagonal prism isomer becomes lower in energy by 0.30 eV. Simi-

larly the Ni-doped hexagonal prism isomer is 0.45 eV lower in energy than the fullerene isomer. The magnetic moment of a Ni atom in the fullerene cage is, however, quenched as the exchange splitting in the Ni atom is small. Therefore, the undoped fullerene cage is lower in energy, but the EE of a dopant is better in the hexagonal prism cage. The competition between the two changes the relative stability of the doped isomers.

As the empty cages have large HOMO-LUMO gaps, the valence electronic states of the metal atom may lie in this gap and affect the properties of the cages. This is found, for example, for Ti-, Cr-, Mn-, and Fe-doped $Si_{12}H_{12}$ cages. The angular momentum decomposition of the wave functions for different electronic states shows that for cases such as $Fe@Si_{12}H_{12}$ there are states of the doped cage that lie in the HOMO-LUMO gap of the empty cage. In most of these cases the symmetry of the cage is reduced and therefore the electronic spectra are more spread. Later we shall discuss the electronic structure for selected clusters.

3. $Si_{14}H_{14}$

Similar to the case of the $n=12$ cage, we find that for the $n=14$ cage also the higher-energy isomer of the empty cage becomes 0.07, 1.18, 0.72, 0.95, 0.32, and 0.24 eV lower in energy for Ti, V, Cr, Mn, Fe, and Pd atom doping, respectively with 2, 3, 4, 3, 2, and $0\mu_B$ magnetic moments. The higher-energy isomer of $Cr@Si_{14}H_{14}$ and $Mn@Si_{14}H_{14}$ have 6 and $5\mu_B$ magnetic moments, which are the same as in the case of free Cr and Mn atoms, respectively. However, in the case of Ni and Zr that are isoelectronic to Pd and Ti, respectively, the lowest-energy undoped isomer is also 0.17 and 0.44 eV lower in energy compared to the higher-energy isomer. These have 0 and $2\mu_B$ magnetic moments, respectively. In some of these cases the two isomers lie close in energy and it is possible that both may exist simultaneously under experimental conditions. Cr and Fe [Fig. 5(h)], as well as Mn [Fig. 5(i)], drift towards the center of the hexagon as for the $n=12$ case. A similar behavior has been found[46] in Mn- and Fe-doped Si nanotubes with hexagonal cross section. Also in the case of the lowest-energy isomer of $Ni@Si_{14}H_{14}$, Ni drifts towards a pentagon while Zr drifts towards an atom along the threefold symmetric axis. The HOMO-LUMO gaps for Cr-, Mn-, and Fe-doped cages in the lowest-energy isomers are 0.72, 0.38, and 0.70 eV while the EEs are 1.78, 1.79, and 3.85 eV (Fig. 6), respectively. Again Cr- and Mn-doped cages have low EEs among these metal atoms and the behavior is similar to $n=10$ and 12 cages. A similar feature was obtained[2] for metal-encapsulated clusters of silicon doped with a Cr atom. However, for Ni doping there is a large HOMO-LUMO gap of 2.07 eV as also in the case of the $n=10$ cage and the EE is 4.64 eV. The HOMO-LUMO gap is also large with the values of 1.74 and 1.07 eV for Pd and V, respectively. However, for Ti and Zr the HOMO-LUMO gap is only 0.55 and 0.16 eV, respectively.

4. Si_nH_n ($n \geq 16$)

The special stability of the $n=16$ and 20 cages makes them attractive for endohedral doping. These cages are large

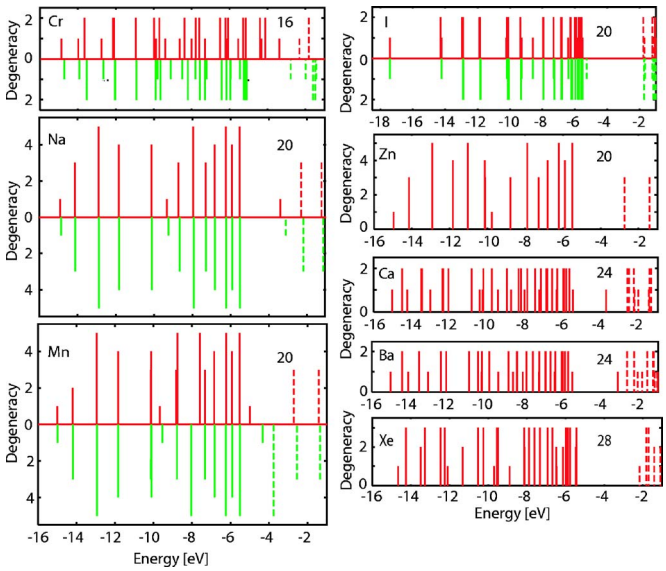

FIG. 7. (Color online) Electronic spectra of selected doped Si_nH_n clusters. The numbers denote the value of n and the element, the dopant. The broken lines correspond to unoccupied states.

enough to accommodate a variety of atoms. Among bigger size atoms we tried rare gases[47] that are interesting because doping of Xe makes[34] clathrates luminescent. We find that the doping of Ar in the $n=16$ cage and Xe in the $n=20$ cage is endothermic by 2.21 and 1.53 eV, respectively. The cost of endohedral doping of Ar in the $n=20$ cage [Fig. 5(m)] reduces to 0.48 eV. Interestingly in the Ar-doped $Si_{20}H_{20}$ cage the HOMO-LUMO gap increases to 3.51 eV from 2.91 eV (PAW). In the case of the $n=24$ cage [Fig. 5(o)], the cost of endohedral doping of Xe and Ar reduces to 0.66 and 0.06 eV, respectively, and the HOMO-LUMO gap increases to 3.20 and 3.06 eV from 2.80 (PAW) eV for the empty cage. In the $n=28$ cage, Xe doping is still slightly endothermic by 0.09 eV, but in the case of Ar, there is a small gain of 0.23 eV, while the HOMO-LUMO gap increases to 3.25 and 3.11 eV for Xe and Ar, respectively from 2.94 eV (PAW) for the undoped cage. In these cases the Pauli repulsion between the closed electronic shells of the cage and the guest atom and consequently the cost of doping reduces with an increase in the size of the cage. As mentioned before, the LUMO of the undoped cage has much weight inside the cage. Therefore when a closed electronic-shell guest atom such as Ar is placed inside the cage, the LUMO level of the empty cage, which remains unoccupied after doping, shifts upwards [see Fig. 7 Xe doping in the $n=28$ cage and compare with Fig. 3(a)] and in some cases the LUMO+1 level of the undoped cage becomes the LUMO of the doped cage. Accordingly both the LUMO and the HOMO of the doped cage will have dominant weight on the cage atoms. The $5s$ level of the guest Xe atom lies at the bottom of the spectrum (not shown in Fig. 7) and the $5p$ states lie around the middle of the occupied region of the spectrum. Most of the states of the cage remain nearly unchanged. The p-type cage states (considering the cage to be nearly spherical) interact with the $5p$ states of the guest atom. The increase in the HOMO-LUMO gap of these doped cages is similar to the case of Xe doping in Si_{46}

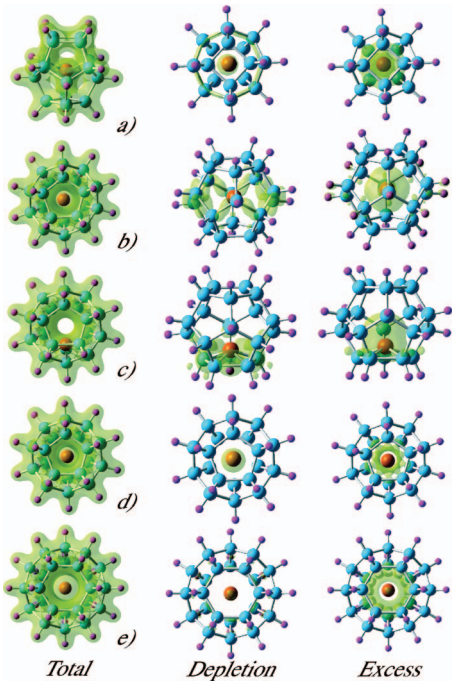

FIG. 8. (Color) Electronic total charge density isosurfaces and the depletion and excess of charge as compared to the sum of the electronic charge densities of the Si_nH_n cage and the dopant atoms at the respective positions in the doped Si_nH_n cages. (a) Cr in $n=16$, (b)–(d) I, Be, and Cr in $n=20$, and (e) Ba in the $n=24$ cage.

clathrates.[34] From our results the doping of Ar is possible in the $n=28$ cage with the dopant occupying the center of the cage [Fig. 5(q)].

An interesting case is the doping of an iodine atom. It occupies the center of the $n=20$ cage with a small EE of 0.39 eV. Iodine represents hole doping of the cage because its 5*s* valence electronic level lies at the bottom of the cage electronic spectrum while the 5*p* level lies below the HOMO of the empty cage states. After doping, iodine valence states are still below the HOMO of the doped cage and are fully occupied making a hole in the HOMO of the empty cage states. This is seen from the electronic-charge density isosurface in Fig. 8(b). There is depletion of charge from the Si cage and an excess of electronic charge around the iodine atom. The hole also leads to a small distortion in the cage from the icosahedral symmetry because in the empty cage the HOMO is fivefold degenerate [Fig. 3(a)]. The latter does not hybridize with the *p* orbitals of iodine but a lower-lying threefold degenerate state of the undistorted cage hybridizes with the *p* orbitals of iodine. The charge transfer from the fivefold degenerate HOMO level of the empty cage to iodine makes the LUMO of the doped cage to lie very close to the HOMO of the doped cage like an acceptor level (Fig. 7). It is followed by a large gap of 3.55 eV as the LUMO of the undoped cage is again pushed up very similar to the case of Ar and Xe discussed above due to the effectively closed-shell nature of I after the charge transfer. Accordingly, this doped specie would have high-electron affinity. The doping of I and similarly other halogens makes this cage behave like a halogen with the hole lying on the cage. There is a net magnetic moment of $1\mu_B$ due to the odd number of electrons.

The other extreme case is the doping by an alkali atom. Among the alkali atoms we find that Na is not bound in the $n=16$ cage but in the $n=20$ cage there is a favorable EE of 0.66 eV. Sodium occupies the center of the cage and the doped cage retains I_h symmetry. There is a net magnetic moment of $1\mu_B$. Its 3*s* electronic level lies ≈ 2 eV above the HOMO of the $Si_{20}H_{20}$ cage within the HOMO-LUMO gap. It forms the HOMO of the endohedral fullerene giving it the character of an electron donor. This can be seen in Fig. 7 from the distribution of the electronic states. The HOMO-LUMO gap is only 0.29 eV because the down-spin state of the Na 3*s* orbital lies close in energy. Sodium interacts weakly with the cage and the electronic states of the cage remain nearly unaffected by doping. There is almost no charge transfer between the Na atom and the cage. Similar results are obtained for $n=24$ and 28 cages with the EE of 0.82 and 0.81 eV, respectively. The higher values of the EE in $n=24$ and 28 cages support the experimental results[48] of the preferential occupation of $n=28$ cages by Na in silicon clathrates for low-doping concentration. Results for other alkali-metal atoms are likely to be similar though the EE is expected to decrease with an increase in the size of the metal atom. It is noteworthy that alkali-metal atom doping has been used in clathrates and the binding energy of the metal atom has been found[49] to be small. The weak binding and rattling of the doped atom in the cage give rise to the low thermal conductivity of the clathrates. The doping of alkali-metal atoms in the fullerene cages makes the doped cages have alkaline character, though unlike halogen doping, the electron remains on the guest atom.

Doping with divalent atoms such as Be, Zn, Ca, and Ba, which have closed electronic shells, is to some extent similar to rare gas atoms. For Be, Ca, and Ba the valence *s* level of the dopant lies within the HOMO-LUMO gap of the cage and the HOMO-LUMO gap becomes small (see, e.g., the energy spectra for Ca and Ba doping in the $n=24$ cage in Fig. 7). As both the cage and the dopant atom are closed electronic-shell subsystems, the EEs of these atoms are again small as shown in Fig. 6. The Berylium atom, being smaller, can be accommodated in the $n=16$ cage, and it lies at the center of this cage [Fig. 5(j)] and the EE is 0.97 eV. The HOMO-LUMO gap of the endohedral cage reduces to 1.48 eV. The larger size of Zn and Ca atoms makes them energetically unfavorable in the $n=16$ cage though the cost is only 0.15 and 0.12 eV, respectively. However, Ba breaks the $n=16$ cage [Fig. 5(l)]. On the other hand, Be in $n=20$, 24, and 28 cages drifts towards the wall of the cage. It occupies the center of a hexagon in the $n=24$ cage [Fig. 5(p)] and caps a pentagon in the $n=20$ and 28 cages [Figs. 5(n) and 5(t)]. Note that in the case of the $n=20$ cage, there are all pentagons. A similar result has been obtained by Zhang *et al.*[20] for the $n=20$ cage. For the $n=28$ cage we also placed a Be atom near a hexagon, but it goes back to a pentagon. The EE of a Be atom in different cages remains small with values of 1.34, 1.47, and 1.24 eV and the HOMO-LUMO gap is 1.16, 1.10, and 1.14 eV for $n=20$, 24, and 28 cages, respectively. The HOMO in these cases arises dominantly from the dopant. In order to further check if there is any charge transfer between the dopant and the cage, in Fig. 8(c) we have shown the charge density for Be in the $n=20$ cage. It shows a slight

depletion of charge from some Si-Si bonds in the vicinity of the Be ion and access of charge around the Be ion and it spills towards the center of the cage.

The large size of the Ba atom makes the doping in the $n=20$ cage also unfavorable but the embedding cost is only 0.11 eV. The HOMO-LUMO gap reduces to 0.4 eV. This is in contrast to the $Ba@Si_{20}$ (without H capping) case in which Ba encapsulation is energetically favorable[50] in the Si_{20} cage with some distortions. This is due to the open-shell electronic structure of Si_{20} that leads to charge transfer from Ba to the cage. Our results of $Ba@Si_{20}H_{20}$ support the formation of Ba-doped clathrates at high pressure. However, there is a gain of 1.52 and 1.28 eV, respectively, when Ca and Ba are doped in the $n=24$ cage. The HOMO-LUMO gap in the two cases is 1.12 and 0.48 eV, respectively. Also Ca doping in the $n=20$ cage leads to a gain of 1.22 eV and the HOMO-LUMO gap is 1.06 eV. In all these cases the guest atom is at the center of the cage. Therefore Ca is favored in both the $n=20$ and 24 cages but Ba is preferred in the $n=24$ cage. Doping of Ca [Fig. 5(s)] and Ba in the $n=28$ cage leads to a gain of 1.41 and 1.61 eV with the HOMO-LUMO gap of 1.35 and 0.79 eV, respectively. Therefore Ba doping becomes even more favorable in the $n=28$ cage than Ca. The electronic charge density of Ba in the $n=24$ cage shows an excess of charge in between the Ba atom and the cage [Fig. 8(e)], which also leads to a higher value of EE. Our results suggest that Ba would prefer to occupy Si_{28} and Si_{24} cages in clathrates, though the Si_{20} cage could also be occupied without costing much energy. In the case of codoping of Na and Ba, it is likely that Na would ocupy the Si_{20} cage leaving the bigger cages for Ba. Interestingly such a behavior has been found[51] experimentally in $Na_2Ba_6Si_{46}$ and $Na_{16}Ba_8Si_{136}$ clathrates.

Among the other divalent atoms, doping of Zn leads to a different behavior. The Zinc atom lies at the center of the cage with a small EE of 0.465, 0.47, and 0.391 eV, respectively, in $n=20$, 24, and 28 [Figs. 5(m), 5(o), and 5(r)] cages. The HOMO-LUMO gaps of the cages remain nearly unchanged and the values for the doped $n=20$, 24, and 28 cages are 2.77, 2.54, and 2.74 eV, respectively. This is because the $3d$ and $4s$ electronic states of the Zn atom lie much below the HOMO of the empty cage Si_nH_n fullerenes and hybridize weakly with the cage states. Therefore the electronic states of the cage are affected little by doping [see Figs. 3(a) and 7]. The $4s$ level of Zn lies below the fivefold degenerate HOMO of the cage while the LUMO of the undoped cage shifts significantly up and the threefold degenerate LUMO+1 becomes the LUMO of the doped cage similar to the case of the doping with rare gases. It has significant hybridization with the $4p$ orbitals of Zn. Therefore in this case, the HOMO belongs to the cage while the LUMO has a mixed character. However, in the case of Zn doping in the $n=16$ cage, the site-decomposed electronic contributions show that the $4s$ level of Zn constitutes the HOMO while the LUMO arises from the cage and the HOMO-LUMO gap remains large with the value of 2.16 eV. Zn doping in the $n=16$ cage is endothermic by 0.15 eV. These results show that the electronic structure of the doped cages can be suitably modified by proper matching of the cage size and the dopant.

Transition-metal atoms could lead to possibilities of developing species with large magnetic moments. Studies[22,23] on a large number of metal-encapsulated silicon clusters show that transition-metal atoms can be accommodated well in cages with $n \geqslant 12$. We have studied doping of many transition-metal atoms such as Ti, V, Cr, Mn, Fe, Co, Zr, Nb, Mo, and W. Our results show that the doped cages have atomiclike large magnetic moments in most cases. Among the transition-metal atoms with high magnetic moments, we find that Mn and Cr atoms in the $n=16$ cage are preferred at the center [Fig. 5(j)] with 2.36–2.40 Å Si-Si and 2.79 Å Si-metal bond lengths, but iron atom drifts slightly towards a pentagon [Fig. 5(k)] with Si-Fe bond lengths of 2.61–2.98 Å. The magnetic moments for the doping of Cr, Mn, and Fe atoms are 6, 5, and $4\mu_B$, respectively, as in the case of the isolated metal atoms with similar occupancies of $3d$ and $4s$ orbitals. The energies of some of these orbitals lie within the HOMO-LUMO gap of the cage (see the energy spectrum of Cr in the $n=16$ cage in Fig. 7). This atomiclike behavior is because the metal atom interacts weakly with the cage and the EE is 0.90, 0.68, and 1.71 eV (Fig. 6) for Cr, Mn, and Fe, respectively. The charge densities for Cr in the $n=16$ and 20 cages [Figs. 8(a) and 8(d)] show small charge depletion from the Si-Si bonds and near the Cr atom while an excess of charge occurs between the Cr atom and the cage. This is in contrast to strong interaction[1] (EE about 10 eV) of a transition-metal atom with the Si_{16} cage (without H capping) that also quenches the magnetic moments of the metal atom. In the $n=20$ cage, M=Cr, Mn, and Fe atoms drift slightly towards the top of a Si atom with M-Si (Si-Si) bond lengths of 3.30 ± 0.07 Å (2.36 Å). The magnetic moments are again atomiclike with the values of 6, 5, and $4\mu_B$, respectively, and the EEs of the metal atoms are 1.19, 1.07, and 1.53 eV. The HOMO-LUMO gaps of the doped cages are significantly reduced and have the values of 0.6, 0.52, and 0.52 for $n=16$ and 0.96, 0.57, and 0.13 eV for $n=20$ cages, respectively. This is because the unoccupied $3d$ states of Fe and Mn become the LUMO for the doped cages. As shown in Fig. 7 for the $n=20$ cage and Mn doping, the $3d$ up-spin state lies about 3.7 eV below the HOMO of the doped cage while the down-spin $3d$ states (fivefold degenerate) are unoccupied and form the LUMO. The $4s$ up- and down-spin states of the Mn atom are occupied and the down-spin $4s$ state forms the HOMO of the doped cage. The I_h symmetry of the cage is largely kept. Particularly for Cr and Mn the $3d$ states remain fivefold degenerate in the icosahedral symmetry. The EEs for Cr and Mn in $n=24$ (0.82 and 1.03 eV) and 28 (0.92 and 0.88 eV) cages are similar. However, the EE of Fe in the 28 cage is 2.65 eV and its magnetic moment is reduced to $2\mu_B$ due to distortions in the cage. We also studied Mo and W in the $Si_{20}H_{20}$ cage as the hybridization with the cage can be expected to be different compared with Cr doping. The EE of Mo and W increases to 1.31 and 1.69 eV, respectively, and the HOMO-LUMO gaps are 0.92 and 0.64 eV. The magnetic moment remains $6\mu_B$. Thus the EE increases as we go down in a column in the periodic table due to increased hybridization of the orbitals of the guest atom and the cage. Further studies of a V atom in the $n=16$ cage give the EE to be 1.73 eV and the HOMO-LUMO gap is 0.45 eV. Interesingly in this case the up-spin $3d$ states of V are fully occupied and it leads to a $5\mu_B$ magnetic moment on the doped cage and 0.32 eV HOMO-LUMO gap. V

drifts away from the center and the Si-V bonds lie in the range of 2.77–3.19 Å. Also for the $n=20$ cage, there is a $5\mu_B$ magnetic moment with the up-spin $4s$ and four $3d$ states being occupied. This also leads to only a 0.03 eV HOMO-LUMO gap as the remaining up-spin $3d$ state becomes the LUMO. Similarly Nb doping also leads to a $5\mu_B$ magnetic moment on the $n=20$ cage, and it is slightly displaced from the center. Nb is slightly bigger in size than V and it behaves similar to V in the $n=16$ cage. The embedding energy of the Nb atom in the $n=20$ cage is 2.12 eV and the HOMO-LUMO gap is 0.49 eV. Zr in the $n=20$ cage has 2.39 eV EE and a $4\mu_B$ magnetic moment. The Zirconium atom has been found to interact strongly with the pure Si_{16} cage and it forms the $Zr@Si_{16}$ fullerene. In the $n=20$ cage it is slightly displaced from the center of the cage and the Si-Si bond lengths are 2.31 ± 0.05 Å. Additionally, there is a small cubic distortion so that the $4d$ level splits into a nearly threefold and a twofold degenerate levels. The up-spin nearly threefold degenerate level and the up-spin $5s$ level (HOMO) are occupied giving rise to a $4\mu_B$ magnetic moment. The down-spin $5s$ electronic level of Zr forms the LUMO and the HOMO-LUMO gap is only 0.26 eV. These examples show that endohedral doping of the transition-metal atoms in hydrogenated Si cages lead to species with high magnetic moments and an atomiclike behavior. In most of the cases of transition-metal doping, the HOMO-LUMO gap is small.

IV. SUMMARY

In summary, we have studied the stability of endohedral hydrogenated Si fullerenes doped with various atoms similar to the case of carbon fullerenes. However, for silicon, the cage is stabilized by H termination. Unlike metal-encapsulated Si fullerenes (without H termination), the embedding energy of the dopants in these hydrogenated cages is small due to weak interaction between the dopant and the cage. We find that in some cases the doping makes a higher-energy undoped isomer to become the lowest in energy after doping. Such a behavior may also exist for carbon fullerenes, in particular, for cases where a few isomers are nearly degenerate. Furthermore, doping of transition-metal atoms in cages has been found to lead to atomiclike high magnetic moments that are interesting for developing magnetic superstructures as the metal atom is nearly isolated. Our results suggest that it should be further possible to have endohedral magnetic fullerenes with f electron depants. The HOMO-LUMO gap in these fullerenes can be tuned by changing the dopant as well as the cage size to obtain desired optoelectronic properties. The HOMO-LUMO gap can range from an infrared region to an ultraviolet range and this property makes these clusters fascinating as a new form of nanosilicon. The character of HOMO and LUMO can also be tailored so that it could arise either from the cage or the guest atom. This could make the endohedral species also attractive for sensor applications as well as for the development of derivatives. Our results should also be helpful in understanding clathrate compounds as well as these could lead to the possibility of other unexplored dopants. Finally, we find a larger HOMO-LUMO gap for Ge cages in which case the character of the LUMO is generally different from the Si cages. While we expect the general conclusions about the behavior of dopants in Ge and Sn cages to be similar to those discussed here, the difference in the cage size as well as the LUMO character could lead to variations, which would be interesting for further study.

ACKNOWLEDGMENTS

V.K. gratefully acknowledges the support and kind hospitality at the Institute for Materials Research, the International Frontier Center for Advanced Materials (IFCAM) and the Center for Interdisciplinary Research, Tohoku University, Research Institute for Computational Science (RICS) AIST, Creative Research Initiative "Sousei" (CRIS) of Hokkaido University as well as the support from NAREGI Nano Science Project at RICS, Ministry of Education, Culture, Sports, Science and Technology, Japan and hospitality at the Institute of Mathematical Sciences, Chennai. We thank the staff of the Center for Computational Materials Science of IMR-Tohoku University for allowing the use of SR8000/H64 supercomputer facilities.

[1] V. Kumar and Y. Kawazoe, Phys. Rev. Lett. **87**, 045503 (2001); **91**, 199901(E) (2003).
[2] V. Kumar and Y. Kawazoe, Phys. Rev. B **65**, 073404 (2002); V. Kumar, C. Majumder, and Y. Kawazoe, Chem. Phys. Lett. **363**, 319 (2002); V. Kumar, Eur. Phys. J. D **24**, 81 (2003); V. Kumar, T. M. Briere, and Y. Kawazoe, Phys. Rev. B **68**, 155412 (2003); V. Kumar, Bull. Mater. Sci. **26**, 109 (2003).
[3] V. Kumar and Y. Kawazoe, Phys. Rev. Lett. **88**, 235504 (2002).
[4] V. Kumar and Y. Kawazoe, Appl. Phys. Lett. **80**, 859 (2002).
[5] V. Kumar and Y. Kawazoe, Appl. Phys. Lett. **83**, 2677 (2003).
[6] V. Kumar, A. K. Singh, and Y. Kawazoe, Nano Lett. **4**, 677 (2004).
[7] V. Kumar and Y. Kawazoe (unpublished).
[8] S. M. Beck, J. Chem. Phys. **90**, 6306 (1989).
[9] H. Hiura, T. Miyazaki, and T. Kanayama, Phys. Rev. Lett. **86**, 1733 (2001).
[10] M. Ohara, K. Koyasu, A. Nakajima, and K. Kaya, Chem. Phys. Lett. **371**, 490 (2003).
[11] X. Zhang, G. Li, and Z. Gao, Rapid Commun. Mass Spectrom. **15**, 1573 (2001); X. Zhang, G. Li, X. Xing, X. Zhao, Z. Tang, and Z. Gao, *ibid.* **15**, 2399 (2001).
[12] K. Koyasu, M. Akutsu, M. Masaaki, and A. Nakajima, J. Am. Chem. Soc. **127**, 4998 (2005).
[13] S. Neukermans, E. Janssens, Z. F. Chen, R. E. Silverans, P. v. R. Schleyer, and P. Lievens, Phys. Rev. Lett. **92**, 163401 (2004).
[14] S. Neukermans, X. Wang, N. Veldeman, E. Janssens, R. E. Silverans, and P. Lievens, Int. J. Mass. Spectrom. **252**, 145 (2006).
[15] E. N. Esenturk, J. Fettinger, and B. Eichhorn, Chem. Commun.

(Cambridge) **2005**, 247.
[16] V. Kumar and Y. Kawazoe, Phys. Rev. Lett. **90**, 055502 (2003).
[17] G. A. Rechtsteiner, O. Hampe, and M. F. Jarrold, J. Phys. Chem. **105**, 4188 (2001).
[18] H. Shinohara, Rep. Prog. Phys. **63**, 843 (2000).
[19] F. Pichierri, V. Kumar, and Y. Kawazoe, Chem. Phys. Lett. **406**, 341 (2005).
[20] C.-Y. Zhang, H.-S. Wu, and H. Jiao, Chem. Phys. Lett. **410**, 457 (2005).
[21] F. Pichierri, V. Kumar, and Y. Kawazoe, Chem. Phys. Lett. **383**, 544 (2004).
[22] V. Kumar, Comput. Mater. Sci. **36**, 1 (2006).
[23] V. Kumar, in *Nanosilicon*, edited by V. Kumar (Elsevier, Amsterdam, in press).
[24] H. Prinzbach, A. Weiler, P. Landenberger, F. Wahl, J. Wörth, L. T. Scott, M. Gelmont, D. Olevano, and B. v. Issendorff, Nature (London) **407**, 60 (2000).
[25] C. W. Earley, J. Phys. Chem. A **104**, 6622 (2000).
[26] Z. Chen, H. Jiao, D. Moran, A. Hirsch, W. Thiel, and P. v. R. Schleyer, J. Phys. Chem. A **107**, 2075 (2003).
[27] D. Moran, H. L. Woodcock, Z. Chen, H. F. Schaefer III, and P. v. R. Schleyer, J. Am. Chem. Soc. **125**, 11442 (2003).
[28] Y. Wang, J. Xu, Z. Cao, and Q. Zhang, J. Phys. Chem. B **108**, 4579 (2004); F. Pichierri, V. Kumar, and Y. Kawazoe (unpublished).
[29] M. Takata, E. Nishibori, M. Sakata, M. Inakuma, E. Yamamoto, and H. Shinohara, Phys. Rev. Lett. **83**, 2214 (1999), and references therein.
[30] K. Hirahara, K. Suenaga, S. Bandow, H. Kato, T. Okazaki, H. Shinohara, and S. Iijima, Phys. Rev. Lett. **85**, 5384 (2000); K. Suenaga, T. Okazaki, C.-R. Wang, S. Bandow, H. Shinohara, and S. Iijima, *ibid.* **90**, 055506 (2003).
[31] T. Guo, R. E. Smalley, and G. E. Scuseria, J. Chem. Phys. **99**, 352 (1993).
[32] T. Kume, H. Fukuoka, T. Koda, S. Sasaki, H. Shimizu, and S. Yamanaka, Phys. Rev. Lett. **90**, 155503 (2003), and references therein; J. S. Tse, S. Desgreniers, Z.-Q. Li, M. R. Ferguson, and Y. Kawazoe, *ibid.* **89**, 195507 (2002), and references therein.
[33] G. S. Nolas and C. A. Kendziora, Phys. Rev. B **62**, 7157 (2000).
[34] D. Connetable, V. Timoshevskii, E. Artacho, and X. Blase, Phys. Rev. Lett. **87**, 206405 (2001).
[35] H. Kawaji, H.-O. Horie, S. Yamanaka, and M. Ishikawa, Phys. Rev. Lett. **74**, 1427 (1995).
[36] G. Kresse and J. Furthmüller, Phys. Rev. B **54**, 11169 (1996); D. Vanderbilt, *ibid.* **41**, 7892 (1990).
[37] J. P. Perdew, in *Electronic Structure of Solids' 91*, edited by P. Ziesche and H. Eschrig (Akademie Verlag, Berlin, 1991).
[38] G. Kresse and D. Joubert, Phys. Rev. B **59**, 1758 (1999); P. E. Blöchl, *ibid.* **50**, 17953 (1994).
[39] M. J. Frisch *et al.*, computer code GAUSSIAN 03 (Revision B.05) (Gaussian, Inc., Pittsburgh, PA, 2003).
[40] V. Kumar, Comput. Mater. Sci. **30**, 260 (2004).
[41] M. O. Watanabe, H. Murakamai, T. Miyazaki, and T. Kanayama, Appl. Phys. Lett. **71**, 1207 (1997); T. Uda, Surf. Rev. Lett. **3**, 127 (1996).
[42] I. Vasiliev, S. Ögüt, and J. R. Chelikowsky, Phys. Rev. Lett. **86**, 1813 (2001).
[43] A. K. Singh, V. Kumar, and Y. Kawazoe, Phys. Rev. B **71**, 115429 (2005).
[44] The calculated values of the HOMO-LUMO gaps using the B3PW91 hybrid functional in the Gaussian program for $n=8$, 10, 12, 14, 16, 20, 24, and 28 cages, respectively, are 4.26, 4.50, 4.12, 4.25, 4.43, 4.49, 4.36, and 4.50 eV for Si using the 6-311+G* basis set and 4.22, 4.48, 4.40, 4.56, 4.90, 4.92, 4.70, and 4.63 eV for Ge using the SDD basis set. The small difference in the trends (such as slightly smaller gaps of Ge cages for $n=8$ and 10 compared with Si cages) could be due to the use of a different exchange-correlation functional in the plane-wave and Gaussian calculations and/or a different basis set for Ge in the Gaussian calculation. However, these calculations do reveal the different behavior of the HOMO-LUMO gap for Ge cages as compared with the band gap in bulk.
[45] H. Kawamura, V. Kumar, and Y. Kawazoe, Phys. Rev. B **71**, 075423 (2005).
[46] A. K. Singh, T. M. Briere, V. Kumar, and Y. Kawazoe, Phys. Rev. Lett. **91**, 146802 (2003).
[47] To test the accuracy of the calculations for rare gas dopants, we computed energies of dimers of Ar and Xe. These were found to be weakly bound. The binding energies for Ar_2 and Xe_2 within PAW-GGA were obtained to be 0.068 eV and 0.017 eV, respectively.
[48] F. Tournus, B. Masenelli, P. Melinon, D. Connetable, X. Blase, A. M. Flank, P. Lagarde, C. Cros, and M. Pouchard, Phys. Rev. B **69**, 035208 (2004).
[49] C. W. Myles, J. Dong, and O. F. Sankey, Phys. Status Solidi B **239**, 26 (2003).
[50] Q. Sun, Q. Wang, T. M. Briere, V. Kumar, Y. Kawazoe, and P. Jena, Phys. Rev. B **65**, 235417 (2002); T. Nagano, K. Tsumuraya, H. Eguchi, and D. J. Singh, *ibid.* **64**, 155403 (2001).
[51] T. Rachi, K. Tanigaki, R. Kumashiro, J. Winter, and H. Kuzmany, Chem. Phys. Lett. **409**, 48 (2005).